

# Nonadditivity of Polymeric and Charged Surface Interactions: Consequences for Doped Lamellar Phases.

O. A. Croze and M. E. Cates

School of Physics, University of Edinburgh  
JCMB King's Buildings, Mayfield Road  
Edinburgh EH9 3JZ, Scotland

November 21, 2018

## Abstract

We explore theoretically the modifications to the interactions between charged surfaces across an ionic solution caused by the presence of dielectric polymers. Although the chains are neutral, the polymer physics and the electrostatics are coupled; the intra-surface electric fields polarise any low permittivity species (e.g., polymer) dissolved in a high permittivity solvent (e.g., water). This coupling enhances the polymer depletion from the surfaces and increases the screening of electrostatic interactions, with respect to a model which treats polymeric and electrostatic effects as independent. As a result, the range of the ionic contribution to the osmotic interaction between surfaces is decreased, while that of the polymeric contribution is increased. These changes modify the total interaction in a nonadditive manner. Building on the results for parallel surfaces, we investigate the effect of this coupling on the phase behaviour of polymer-doped smectics.

## 1 Introduction

Many processes in soft and biological systems take place in water and involve the interaction of fatty components, such as membranes or macromolecules. The polar nature of the aqueous environment means these components often acquire surface charges, so that electrostatics plays a key role in determining their physical behaviour. The subject has undergone a substantial revival recently, especially because of its biological relevance [1].

The description of such electrostatic systems generally invokes a continuum approximation (see, e.g., Kjellander in [1]): the electrostatic properties of the solvent (water) and of all uncharged components are accounted for via their electrical permittivity. Membranes in water, for example, have been usefully modelled as dielectric films of low permittivity residing in a high permittivity medium [2, 3]. In general, any dielectric components present, even if neutral, will be involved in modulating electrostatic interactions, because of their polarisation in the electric fields generated by the charged components of the system. This creates nonadditivity, which is not always recognised. Specifically, in modelling neutral polymers between charged surfaces, the electrostatic and polymeric contributions to the intersurface forces are usually treated as independent (see, e.g., sec. 10.7 of [4]). With charged polymers (polyelectrolytes or polyampholytes), their effects on fields is often

attributed solely to the polymer charges, neglecting the dielectric backbone [5]. An exception is the work of Khokhlov et al. [1], in which the polarisation of polyelectrolytes is explicitly included in a description of their adsorption onto an oppositely charged surface. Dielectric phenomena are also well known to be implicated in the distribution of electrolytes in the neighborhood of proteins [6].

In this paper we directly address the interdependence of the polymer physics and electrostatics when charged surfaces interact across solutions of neutral polymers. To gauge the extent of the nonadditive “coupling effects”, we have constructed a simple mean field model which includes such coupling, and calculate the force between charged surfaces across a neutral polymer solution. The model is then adapted to predict the phase behaviour of polymer-doped lamellar phases. Recent investigations of these composite liquid crystals have shown that a substantial amount of polymer can be incorporated in the lamellar phase and can induce phase separation (see [7] and references therein). The polymer has been found to reside either within the bilayers [8, 9] or within the water layers; in the latter case it may adsorb onto the bilayers [10, 11, 12] or it may not [13, 14, 12]; this depends on the local polymer–bilayer interaction. Without charges, the problem provides an experimental realisation of the textbook example of a polymer solution confined in a slit [13, 15]. Most lamellar phases are charged, however. Some existing descriptions correctly recognise that polymers can affect electrostatic interactions by reducing the effective permittivity of the solution confined between bilayers [16, 17, 18, 19], but ignore the feedback of the electrostatics on the distribution of polymer segments themselves. A fully consistent description must either address this, or give a good reason to neglect it. Below we explore this issue further. For simplicity our work is restricted to the case of nonadsorbing polymers whose monomer density vanishes at either of the confining walls.

The paper is organised as follows. Section 2 describes our mean field model and how it can be used to investigate the properties of polymer-doped lamellar phases. The results of our model are then presented and discussed. In Section 3 we show how, for experimentally reasonable parameters, an account of coupling modifies the variation of both the electrostatic potential and the polymer concentration between surfaces of fixed separation. As a result of these changes, the osmotic interaction between the plates is also modified with respect to the uncoupled results from the same model. With the mapping described in Section 2, the osmotic pressure can be used as an equation of state to predict the phase behaviour of doped lamellar phases. The details of this procedure and the results of parameter variation for the phase behaviour of doped smectics are presented and discussed in Section 4. Section 5 discusses the relation to experiment and in Section 6 we draw our conclusions.

## 2 Model

We consider a solution of neutral polymers, confined between charged surfaces (Fig. 1) and contacting a reservoir with which it can exchange heat, polymer chains and electrolyte (salt). By virtue of the surface counterions and the salt ions, the solution is electrolytic and screens the charged surfaces. Since the polymers are nonadsorbing, their monomer density vanishes at both plates.

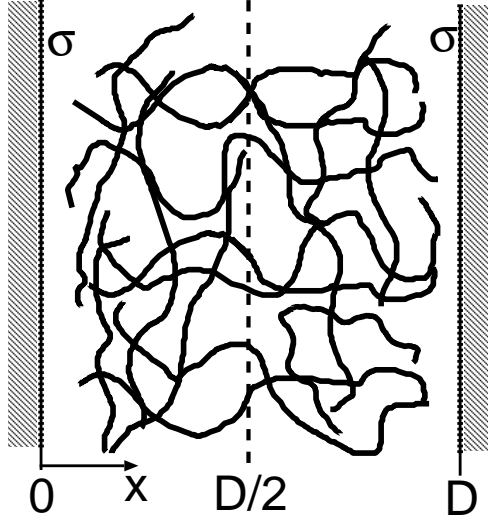


Figure 1: The situation modelled: an ionic solution of nonadsorbing neutral polymers confined between charged surfaces, separated by a distance  $D$  and bearing a surface charge density  $\sigma$ . The ions in solution with the polymers are not shown for clarity. Also not shown is the electrolyte and polymer reservoir with which the system is in equilibrium.

## 2.1 Variational Formulation

With these premises, the free energy characterizing the system is the grand potential  $\Omega(\Gamma, T, \mu_i, \mu_p)$ , minimised at equilibrium when the solution's volume,  $\Gamma$ , its temperature,  $T$ , and chemical potentials,  $\mu_i$  ( $i = +, -$ ) for the ions and  $\mu_p$  for the polymer, are fixed.  $\Omega$  comprises energetic and entropic contributions from the polymer solution, the ions and electrostatics. Adopting a mean field approach, such contributions are conveniently expressed in terms of the monomer volume fraction  $\phi(\mathbf{r})$ , the ion number density  $n_i(\mathbf{r})$  and the electrostatic potential  $V(\mathbf{r})$ . As indicated, these variables are expected to vary with position  $\mathbf{r}$  between the surfaces, so that the free energy needs to be expressed as a density functional, the null variations of which yield the equations of our model. Because the electrostatic potential and the ion densities are not independent variables, but are constrained to obey the Maxwell equation  $\nabla \cdot (\epsilon \nabla V) = -\sum_i n_i q_i$  (where  $q_i$  is the ion charge), it is convenient to adopt the variational formulation of electrostatics [20] to write the free energy as an “action”:

$$\mathcal{F}_\Omega = \int_\Gamma f_\Omega(\mathbf{r}) d\mathbf{r} = \int_\Gamma \{f_{poly}(\mathbf{r}) + f_{ions}(\mathbf{r}) + f_{el}(\mathbf{r})\} d\mathbf{r} \quad (1)$$

The stationary value of this action is identical to  $\Omega$ , as indicated by the subscript. The integrand  $f_\Omega$  is an “action density” which has been expressed as a sum of polymeric ( $f_{poly}$ ), ionic ( $f_{ions}$ ) and electrostatic ( $f_{el}$ ) contributions.

To describe the polymer contribution we adopt the square gradient approximation (SGA) [21]. In this approximation the local free energy density of a polymer solution is given by the reference free energy of the solution at position  $\mathbf{r}$  plus a square gradient term accounting for the nonlocal effects of concentration fluctuations on chain entropies. We choose the Flory–Huggins expression

[22] on a cubic lattice as the reference free energy. The polymer contribution to  $f_\Omega$  is thus:

$$f_{poly}(\mathbf{r}) = \frac{T}{a^3} \left[ \frac{\phi}{N} \ln \frac{\phi}{N} + (1 - \phi) \ln(1 - \phi) + \chi \phi(1 - \phi) - \frac{\mu_p}{T} \phi \right] + \frac{T}{36a} \frac{(\nabla \phi)^2}{\phi} \quad (2)$$

where  $T$  is the temperature of the solution,  $a$  is the lattice parameter of a cubic lattice,  $\phi$  is the monomer volume fraction defined on such a lattice,  $N$  is the number of monomers in a chain,  $\chi$  is the Flory interaction parameter, and  $\mu_p$  is the monomer chemical potential, which is fixed by the reservoir. The coefficient of the square gradient term derives from a comparison of the small fluctuation limit of the SGA with the large wavelength limit of the free energy expansion of a polymer solution in the random phase approximation (RPA) [15, 23, 24]. The ionic contribution, as in Poisson–Boltzmann (PB) theory [1], comprises an entropic “ideal gas” term and a chemical potential term added to ensure ion density conservation:

$$f_{ions}(\mathbf{r}) = T \sum_{i=+,-} n_i (\ln n_i - 1) - \sum_{i=+,-} \mu_i n_i \quad (3)$$

where  $n_i$  is the number density of ionic species  $i = +, -$ , and  $\mu_i$  and  $T$  are respectively the chemical potential of species  $i = +, -$  and the temperature of the system, fixed by the reservoir. As in standard PB theory [1], we consider a dilute solution of pointlike ions. We thus ignore all steric effects associated with finite ion size. This is a good assumption since we are interested in the qualitative behaviour of small ions residing in a polymer solution which may be reasonably concentrated (see Section 3), but is sufficiently far from a melt that any steric reduction of the ion entropy by the polymer can be safely ignored.

The electrostatic contribution to the free energy action is:

$$f_{el}(\mathbf{r}) = \sum_{i=+,-} n_i q_i V - \frac{1}{2} \epsilon_e(\phi) (\nabla V)^2 \quad (4)$$

where  $q_i = z_i e$  is the charge of species  $i$  with valence  $z_i$ , and  $V$  is the electrostatic potential. Equation (4) represents the variational formulation of electrostatics [20]: Poisson’s equation follows from the variation  $\delta \mathcal{F}_{el} = \int_\Gamma f_{el} d\mathbf{r} = 0$  and if its solutions are substituted in (4), the electrostatic energy of the system follows [20]. Throughout these equations we have set  $k_B = 1 = \epsilon_0$ .

The dielectric nature of the polymer solution is accounted for via the effective permittivity  $\epsilon_e$ , which is a function of the monomer concentration  $\phi(\mathbf{r})$  at  $\mathbf{r}$ . The polymer solution is thus treated as a dielectric mixture of solvent with permittivity  $\epsilon_1$  and “dielectric monomers” with permittivity  $\epsilon_2$ . Since the mean field treatment of mixtures with spherical inclusions is particularly simple, we assign a spherical dielectric volume with characteristic radius  $a_d$  to each monomer, as shown in Fig. 2. In general, we expect  $a_d$  to differ from the cubic lattice length  $a$  by an unknown factor  $\gamma$  that depends on the local chain geometry, so that  $a_d = a/\gamma$ . We can now use the Maxwell–Garnett equation for the effective permittivity of a mixture with spherical inclusions [25]:

$$\epsilon_e(\phi) = \epsilon_1 \left( 1 - \frac{3K\alpha\phi}{1 + K\alpha\phi} \right) \quad (5)$$

Here  $K \equiv (\epsilon_1 - \epsilon_2)/(2\epsilon_1 + \epsilon_2)$  is the Mossotti factor. The coefficient  $\alpha \equiv (4/3)\pi/\gamma^3$  accounts for the difference between the volume of a cubic cell of the lattice and that of the effective dielectric sphere each of which models, in its own fashion, a single monomer.

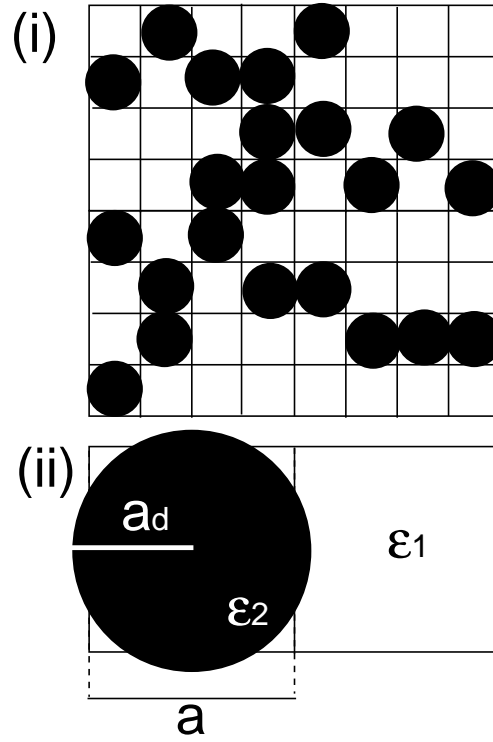


Figure 2: (i) The Flory–Huggins model on a cubic lattice, here represented by a two dimensional square lattice. (ii) Closeup of two cells of the lattice. A dielectric sphere of permittivity  $\epsilon_2$  and radius  $a_d \neq a$  is associated with each occupied site. The surrounding solvent has the same permittivity  $\epsilon_1$  of a pure electrolytic solution. The relation between  $a_d$  and  $a$  is discussed in the text.

Effective medium approaches, such as that leading to Equation (5), involve averaging the electric and displacement fields over a region containing discrete inclusions. When such averaged fields are used in place of the real “microscopic” fields, the medium can be properly characterised by an effective permittivity. This will be a smooth function provided the averaging volume is large enough to contain several inclusions [26, 27]. Thus Equation (5) is strictly valid only if  $R \gg a\phi^{-1/3}$ , where  $R$  is the radius of a spherical averaging volume, containing inclusions of size  $a$  and number concentration  $\phi/a^3$ . If the electric field itself is not mesoscopically uniform but varying on some length scale  $\lambda$  (in our case the Debye length), we also require  $\lambda \gg R$ , so that the field which is being averaged does not change in magnitude over the averaging volume itself.

Aside from this, our model is subject to the same approximations as the Poisson–Boltzmann and Flory–Huggins mean field theories. In particular, the mean field approximation implies that all fluctuation-induced effects are ignored and that the theory is strictly inapplicable to dilute or semi-dilute polymer solutions in good solvents, where Flory–Huggins fails; however we expect it to give a reasonable account of the global picture. On top of this, use of the square gradient approximation requires externally induced concentration variations (and therefore the inducing external fields) to be slowly varying. Another tacit assumption is that the direct effect of ions on the solvent–monomer interactions expressed by the Flory  $\chi$  parameter is negligible; this might not be true in the presence of complexation between chain and ion but should be adequate otherwise.

### 2.1.1 Model Equations

The model’s equations follow from the requirement that Equation (1) be stationary with respect to variations in  $\phi$ ,  $n_i$  and  $V$  (Appendix A). With the additional simplifying assumption that all the ions in solution are monovalent and with the substitution  $\phi = \psi^2$  for the polymer concentration variable, the equations read:

$$\nabla \left[ \tilde{\epsilon}_e(\psi) \nabla \left( \frac{eV}{T} \right) \right] = \kappa^2 \sinh \left( \frac{eV}{T} \right) \quad (6)$$

$$\begin{aligned} \frac{a^2}{9} \nabla^2 \psi &= \frac{3}{2} \frac{K\epsilon_1 \alpha a^3}{T} (\nabla V)^2 \frac{\psi}{(1 + K\alpha\psi^2)^2} + \\ &+ \frac{\psi}{N} \ln \left( \frac{\psi^2}{\psi^r} \right) - \psi \ln \left( \frac{1 - \psi^2}{1 - \psi^r} \right) - 2\chi(\psi^3 - \psi^r \psi) \end{aligned} \quad (7)$$

where  $\tilde{\epsilon}_e \equiv \epsilon_e/\epsilon_1$  is given by the Maxwell–Garnett Equation (5),  $\kappa \equiv \sqrt{2n_s^r e^2/\epsilon_1 T}$  is the inverse Debye length for a monovalent salt of number density  $n_s^r$ , and the superscript  $r$  indicates reservoir values of salt or polymer concentrations.

Equation (6) is the Poisson–Boltzmann equation with a permittivity that depends on polymer concentration and hence on position. Equation (7) describes the concentration variations of a dielectric polymer solution. Similar mean field descriptions of polyelectrolyte adsorption [5, 28, 1] and its effect on surface interactions [5, 28] have been carried out. Like the latter, Equations (6) and (7) describe the concentration variations of a polymer solution next to charged walls. However, since we are not modelling charged polymers, the polymer profile described by (7) is only electrostatically affected because of the dielectric nature of the polymers (described by the first term on the right hand side of (7), which derives from the Maxwell–Garnett relation). Conversely, in Equation (7) the polymer enters only through the modified permittivity.

The influence of confining charged surfaces is incorporated into boundary conditions on Equations (6) and (7). Assuming that the surfaces are parallel, flat, homogeneous and infinite reduces our problem to one dimension. We shall denote the position variable by  $x$ , with origin on the “leftmost” surface ( $x = 0$ , as shown in Fig. 1).  $D$  indicates the separation between the surfaces (the “rightmost” surface is located at  $x = D$ ). For simplicity we have chosen nonadsorbing polymers, and also now choose identical surfaces with fixed surface charge; these choices translate into the following boundary conditions:

$$V'(0) = -\frac{\sigma}{\epsilon_1} = -V'(D) \quad (8)$$

$$\psi(0) = 0 = \psi(D) \quad (9)$$

where the primes mean  $d/dx$ . The fixed surface charge condition was chosen in view of describing charged lamellar phases, whose unknown surface charge density can be estimated from the area available to charged surfactant groups. (It would also be possible to impose fixed surface potential, but this is more complicated numerically and we do not attempt it here.)

The solution of Equations (6) and (7), subject to Equations (8) and (9), allows evaluation of the force per unit area acting between surfaces in the presence of polymer. This is the ‘net osmotic pressure’  $\Pi^{net} = \Pi - \Pi^r$ , defined as the osmotic pressure of ions and polymers on the midplane,  $\Pi$ , less that in the reservoir,  $\Pi^r$ . Note that on the midplane, and also in the reservoir, the local osmotic pressure equates to the normal ( $xx$ ) component of a stress tensor  $\Sigma_{\alpha\beta}$  that elsewhere includes the Maxwell stress arising from electric fields. The Maxwell stress vanishes in the reservoir, and on the midplane by symmetry, which is why the normal force can be equated to the net osmotic pressure there. To find  $\Pi$ , we first show in Appendix A that the stress component  $\Sigma_{xx}$  is independent of  $x$ . Evaluating this (on the midplane for convenience) as a function of plate separation  $D$  gives  $\Pi(D)$  and hence  $\Pi^{net}(D)$ . From Equation (27) of Appendix A, evaluated at the midplane  $x = D/2$ , we finally obtain:

$$\begin{aligned} \Pi^{net}(D) = & 4n_s^r T \sinh^2 \left( \frac{eV|_{D/2}}{2T} \right) - \frac{T}{a^3} \left[ \frac{\phi|_{D/2}}{N} \ln \frac{\phi|_{D/2}}{\phi^r} + \frac{(\phi^r - \phi|_{D/2})}{N} + \right. \\ & \left. + (1 - \phi|_{D/2}) \ln \left( \frac{1 - \phi|_{D/2}}{1 - \phi^r} \right) - \chi(\phi^r - \phi|_{D/2})^2 - (\phi^r - \phi|_{D/2}) \right] \end{aligned} \quad (10)$$

Equation (10) includes both ionic and polymeric contributions to the net pressure: the first term on the right hand side of the equation and the term in square brackets, respectively. The ionic contribution is always repulsive (as one would expect from a mean field treatment of the electrostatics). The polymeric contribution, however, can become attractive at surface separations which unfavourably confine the polymer (values of  $D$  such that  $\phi|_{D/2} < \phi^r$ ). We find below that the interplay of such opposing forces can lead to phase separation, analogous to the liquid–gas transition of ordinary fluids. At mean field level, this shows up as a characteristic  $S$ -shaped loop in the net osmotic pressure (like that of the isotherms predicted by the Van der Waals equation of state [29]). Our model can thereby be used to predict the equilibria of lamellar phases, which are known to phase separate when polymer is added to them (see [7] and references therein).

## 2.2 Mapping onto Lamellar Phases

A lamellar phase consists of a periodic one dimensional crystal of repeating units. Each unit comprises a bilayer of width  $\delta$  and an adjacent solvent layer of width  $D$ , so that the crystal's repeat distance is  $D + \delta$ . Consider a lamellar phase containing  $N_b$  bilayers in contact with a polymer and ion reservoir via a membrane impermeable to the bilayers. The solvent layers of such a phase can be modelled as a polymer solution confined between flat parallel surfaces; a situation described by the model we have just built. This mapping, shown in Fig. 3, is reasonable for lamellar phases with rigid bilayers (so that the surfaces are approximately flat and  $D$  is well defined). Further, since our model does not account for other known forces between bilayers (dispersion, hydration, Helfrich etc.) the mapping is strictly valid only when electrostatics and polymer-induced forces dominate.

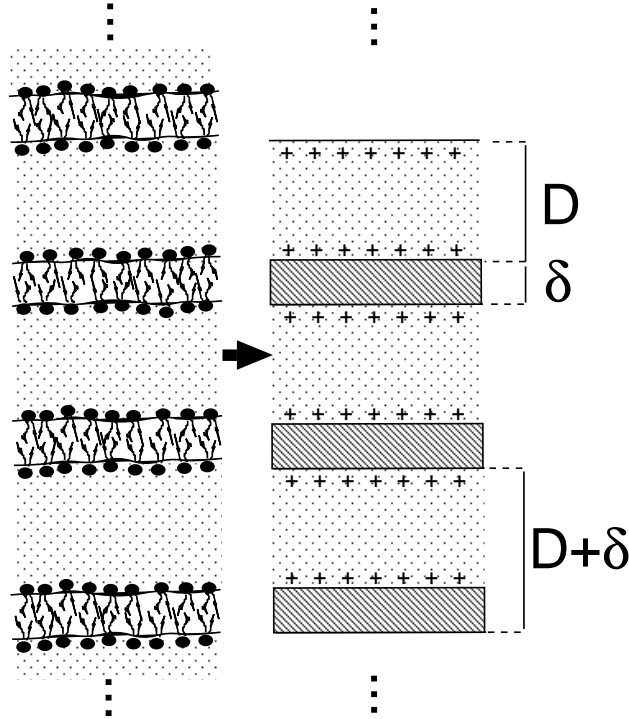


Figure 3: A polymer-doped lamellar phase containing  $N_b$  bilayers, approximated by a periodic succession of units. Each unit comprises a polymer solution confined between charged parallel planes (as described by our model) and a rigid rectangular slab (the bilayer).

Under these assumptions our model can predict the thermodynamic behaviour of a lamellar phase, which is entirely determined by the free energy of the solvent slab. Since pressure is an intensive thermodynamic variable, the osmotic pressure of the lamellar phase is identical to Equation (10); this is the equation of state of the lamellar phase, and determines its phase behaviour.

## 3 Results: Parallel Surfaces

In what follows we give results from the numerical solution to our model. Table 1 displays the “baseline parameters” used in numerical evaluations, all but one of which will be held fixed at the



values shown while the one remaining parameter is varied. The baseline values are loosely based on experimental systems [14, 30, 17, 12, 18]: typical charged bilayers (e.g. CPCl or SDS mixed alcohol) in an aqueous salt solution of water-soluble polymers (PVP or PEG) at room temperature. However, particular parameters were adjusted to have values which might enhance the effects of dielectric coupling, creating on purpose a ‘worst case’ scenario for the additive approximation [31].

Temperature	$T$	298 K
Permittivity of ionic solution	$\epsilon_1$	78.5
Permittivity of polymer	$\epsilon_2$	2
Dielectric factor	$\gamma$	1.5
Polymer lattice length	$a$	10 Å
Flory Parameter	$\chi$	0.495
Number of lattice units per chain	$N$	2000
Surface charge density	$\sigma$	$0.1 \text{ e nm}^{-2}$
Reservoir salt concentration	$c_s^r$	0.02 M
Reservoir monomer volume fraction	$\phi^r$	0.3

Table 1: Values of the parameters used in the numerical evaluation of the model equations and the subsequent determination of phase diagrams. The Debye length in the reservoir corresponding to the salt concentration shown above is  $\lambda = 21.5 \text{ Å}$ .

To maximise dielectric contrast, a value of 2 (the permittivity of hydrocarbon oils) is chosen for the polymer permittivity  $\epsilon_2$ . Similarly, the  $\chi$  parameter is set near the *theta* point, enhancing the susceptibility of the polymer to external fields. Our choice of  $\gamma$ , the size difference between the lattice length and the radius of the dielectric sphere, is likewise made to enhance coupling effects. Physically, the dielectric size of a lattice monomer depends on how many ‘‘oily’’ hydrocarbon groups are contained in the backbone or side groups of every chemical monomer. How much bigger the dielectric volume occupied by the polymer is with respect to the steric volume is hard to estimate precisely. Our choice of  $\gamma = 1.5$  entails that the Flory–Huggins (‘‘entropic’’) volume available to a lattice monomer,  $V_{FH}$ , occupies about 80% of the polarisable volume,  $V_d$  ( $V_{FH}/V_d \simeq \gamma^3/4 \approx 0.8$ ). The lattice length  $a$  is modelled on the water soluble polymer PVP. As shown in [32],  $a$  can be related to the chemical monomer size,  $l$ , of the polymer of interest and the polymer molecular weight,  $M_w$ , to the number  $N$  of lattice units per chain. On a cubic lattice, one finds  $a = 10 \text{ Å}$  and  $N = 2000$  for PVP with  $l \simeq 30 \text{ Å}$  and  $M_w \simeq 500000$ . (Note that the  $N$  is not an important control parameter in the parameter regime of interest to us.) Finally the reservoir monomer concentration was chosen at a reasonably high value of  $\phi^r = 0.3$  so that the concentration of polymer would not be too small, swamping out any dielectric coupling effects.

Given these ‘‘worst-case’’ choices, the uncoupled theory gives a surprisingly good approximation to the full one in most cases. To a significant extent, this justifies the assumption of additivity, tacitly made by some authors [4], and inconsistently justified by others [16, 17]. However, we are not aware of any simple order-of-magnitude arguments that can explain this without pursuing the more detailed calculations presented here.

### 3.1 Potential and Polymer Concentration Profiles

Fig. 4 displays the dimensionless electrostatic potential  $W \equiv eV/T$  and monomer concentration profile  $\Phi \equiv \phi/\phi^r$  as a function of dimensionless position  $X \equiv x/\lambda$ , for surfaces separated by  $D/\lambda \simeq 2.37$  (recall  $\lambda$  is the Debye length defined in the reservoir). The solutions to the full model (coupled equations) were obtained using an adaptation of the shooting method [33] to solve the Equations (6) and (7) subject to the boundary conditions (8) and (9). For comparison, the solutions found in the additive approximation (uncoupled equations) are also presented.

Qualitatively, the solutions of the two descriptions are similar. The “coupled” electrostatic potential displays the characteristic symmetric shape of the solutions to the standard Poisson–Boltzmann equation (uncoupled case); similarly, the monomer concentration profile compares well with the predictions of a mean field description of nonadsorbing polymer chains confined in a slit [34]. The characteristic depletion of monomers from between the surfaces can be observed in both cases. It is well known that the pressure imbalance created by such depletion can cause the surfaces to attract, if the polymer solution is sufficiently squashed that it escapes from between the plates, reducing the osmotic pressure there.

The results, however, also highlight the interesting features which follow from a full account of the polymers’ dielectric properties. First, the electrostatic potential is reduced around the midplane (where the polymer monomers are more concentrated) with respect to the uncoupled solutions. The reduction is due to the additional electrostatic screening provided by the monomers because of their polarisation. Second, the monomer concentration profile displays an increased depletion from the surfaces. This is also a consequence of polarisation and results from the electrostatic energy penalty of placing dielectric monomers in the surface fields.

### 3.2 Osmotic Pressure Between Parallel Surfaces

Fig. 5 displays the predicted variation (coupled and uncoupled cases) of total osmotic pressure between surfaces of dimensionless surface separation  $D/\lambda$ . Both descriptions predict a van der Waals loop. However, in the coupled picture the loop is translated to lower pressures and slightly larger separations with respect to the uncoupled, additive case. In addition, while at very small separations coupled and uncoupled profiles coincide, at large separations dielectric coupling lowers the osmotic pressure curve below the additive prediction.

To understand these differences the ionic and polymeric contributions to the midplane pressure are also shown in Fig. 5. For both models, the ionic contribution is always repulsive, whilst the polymeric contribution is attractive for separations below those at which the polymer starts to be expelled from between the plates. However, for distances large enough that no significant amount of polymer has been expelled, the ionic contribution to the coupled pressure profile decays more rapidly than the uncoupled prediction. This stems from the more efficient screening of the electrostatics in the presence of dielectric monomers. Another effect of the dielectric coupling is that the polymer contribution becomes attractive at larger  $D/\lambda$  than the uncoupled one. This represents an “electrostatically enhanced” depletion of polymer from the surfaces as the dielectric monomers are expelled from the high-field regions near the confining plates.

We can thus summarize the overall differences between the net pressure profiles: at large distances the shorter range of the coupled electrostatic repulsion lowers the pressure profile with respect to the uncoupled prediction; the larger range of the polymer expulsion then promotes the occurrence of the van der Waals loop; finally, at small enough separations the polymer is fully

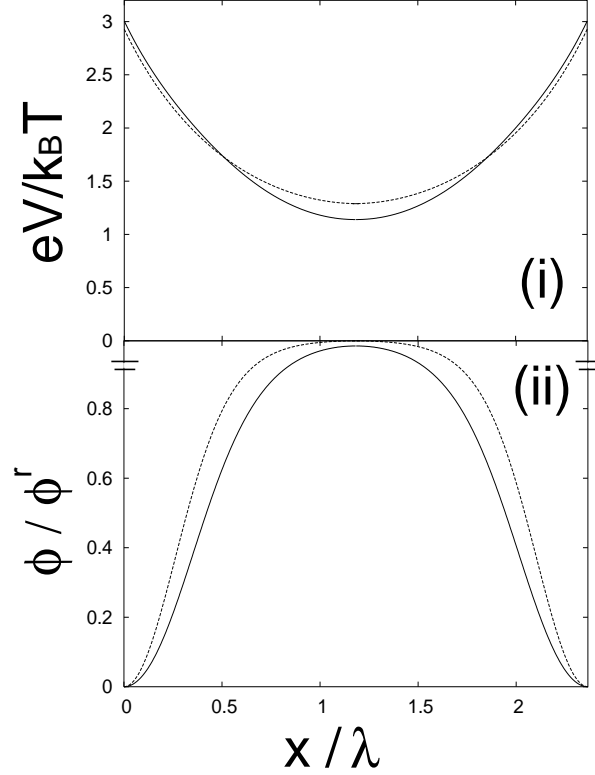


Figure 4: Plots of the numerical solutions of Equations (6) and (7) subject to the boundary conditions (8) and (9), for a surface separation is  $D \simeq 2.37\lambda$ , and using the parameters of Table 1. The results display both coupled (solid line) and uncoupled (dotted line) solutions for (i) the dimensionless electrostatic potential,  $eV/k_B T$ , and (ii) the monomer concentration rescaled by the reservoir value,  $\phi/\phi^r$ , as functions of the dimensionless position between surfaces,  $x/\lambda$ .

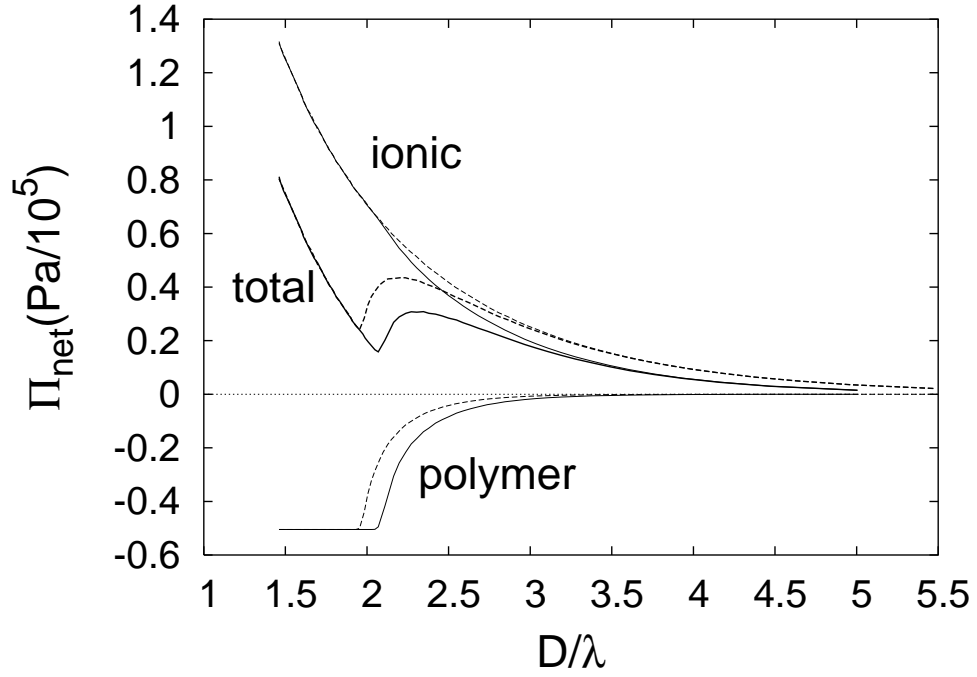


Figure 5: Net osmotic pressure as a function of  $D/\lambda$ , together with its ionic and polymeric contributions. The plots were obtained from Equation (10) by substituting the midplane values of  $V$  and  $\phi$  from the solutions of (6) and (7) for various  $D$ . The coupled (solid lines) and uncoupled (dashed lines) cases are shown. Parameters as in Table 1.

expelled, the dielectric coupling is removed, and coupled and uncoupled predictions coincide.

## 4 Results: Phase Diagrams

### 4.1 Expected Phase Behaviour

As mentioned in the Introduction, the addition of polymer to charged lamellar phases has experimentally been observed to induce phase separation. X-ray scattering studies on these systems have mainly evidenced two kinds of separation [10, 14]:  $L_\alpha L_\alpha$  coexistence between two lamellar phases with different spacings, and  $L_\alpha L$  coexistence between a single lamellar phase and an isotropic solution of polymer (with trace surfactant). The occurrence of phase separation and its modality depend, if all other parameters are held fixed, on the relative composition of the prepared mixture. This has been usefully mapped on density–density phase diagrams plotting the polymer content of the sample against its surfactant composition (e.g. [10, 12]).

### 4.2 Predicting Phase Coexistence

We can explain the phase behaviour just described using our model’s equation of state, Equation (10). Recall that in mean field theories like ours, phase coexistence shows up as a Van der Waals loop in plots of the net osmotic pressure as a function of bilayer separation  $D$ . To deal with this we can deploy the Maxwell construction [29], finding a horizontal line which cuts the van der Waals loop into two regions of equal area (Fig. 6). The horizontality of the line represents the equality of pressures for coexisting phases of different spacings  $D$ , whereas the equal areas represent the equality of chemical potentials [29]. The coexistences found in this way connect two lamellar phases of different layer spacings ( $L_\alpha L_\alpha$  coexistence). This type of coexistence only occurs for a positive pressure: referring to Fig. 5, the polymer-induced attraction causes phase separation, but cannot overcome the electrostatic repulsion between bilayers.

However, when the polymer contribution is large enough, the pressure can become negative and a special type of Van der Waals loop occurs across the zero-pressure axis (Fig. 7). This amounts to a coexistence between a lamellar phase of finite  $D$ , found where the pressure profile crosses the zero axis, and a lamellar phase of infinite  $D$  (identical to the reservoir) which is represented asymptotically by the pressure tending to zero at infinite  $D$ . Hence this modified construction allows the prediction of  $L_\alpha L$  coexistence. However, the resulting areas are not equal in general; this is because the chemical potential of the surfactant is undefined in the bilayer-free state of infinite  $D$ . Recalling that the Maxwell construction is equivalent to the common-tangent construction on the Helmholtz free energy, the failure to equate chemical potentials under these conditions corresponds to the so-called ‘virtual tangency’ condition in which a phase at finite surfactant density connects with one at zero density [35]. A more accurate treatment would allow for the finite molecular or micellar solubility of surfactant in water, giving a slightly more elaborate calculation (in which the slope of the free energy is rapidly varying at very low surfactant concentration) but an almost identical result for the coexistence properties.

Thus, using the reservoir monomer concentration to control the polymer content of our lamellar phase, Equation (10) allows us to determine the equilibrium spacings  $D$ . The relation between bilayer volume fractions  $\phi_b$  and separations  $D$  follows from simple geometry:

$$\phi_b = \frac{\delta}{D + \delta} \quad (11)$$

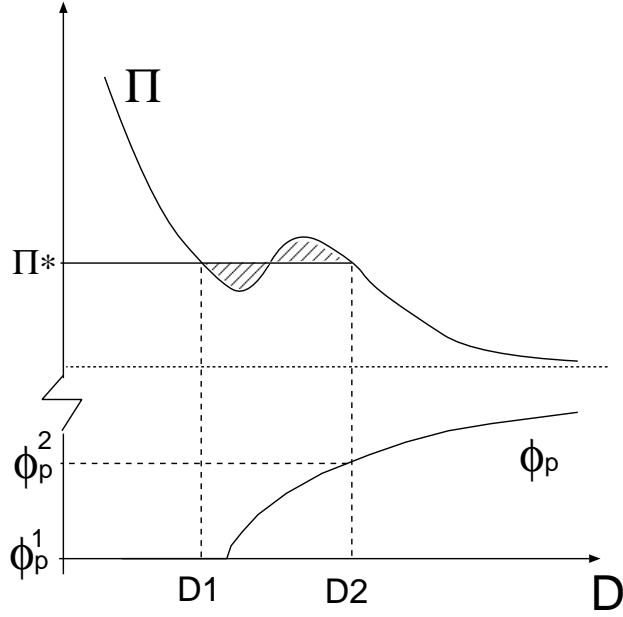


Figure 6: The Maxwell construction for the osmotic pressure (10) of a polymer doped lamellar phase, predicting  $L_\alpha L_\alpha$  coexistence at spacings  $D_1, D_2$ . Once these spacings are identified, the corresponding polymer content of coexisting phases can be obtained from a graph of Equation (12), as shown.

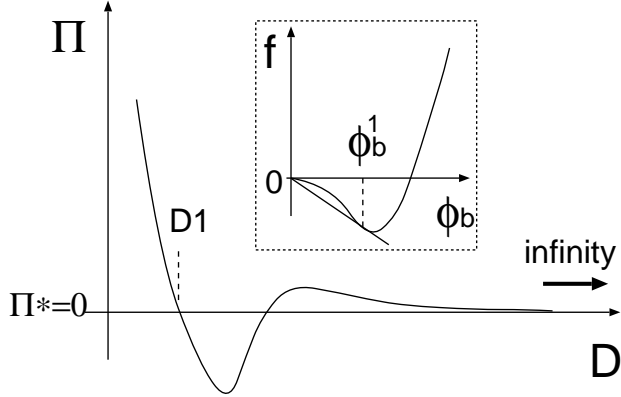


Figure 7: The special Maxwell construction for  $L_\alpha L$  coexistence. The isotropic fluid is represented by a putative lamellar phase with  $D = \infty$  and hence zero osmotic pressure. In reality an exponentially small amount of surfactants coexisting with the lamellar phase resides in the reservoir. The inset shows the equivalent condition of virtual tangency, when the common tangent construction is used to determine phase equilibria from the free energy density  $f$  as a function of volume fraction  $\phi_b$ ; see [35].

Where we recall  $\delta$  is the bilayer thickness. Similarly, the bulk polymer volume fraction  $\phi_p$  within a lamellar phase is found by integrating the polymer profile  $\phi_p(x) \equiv \psi^2(x)$  (from the solution of Equation (7)) for a given  $D$ , normalising by the full volume now including the bilayers themselves:

$$\phi_p = \frac{1}{D + \delta} \int_0^D \phi_p(x) dx \quad (12)$$

### 4.3 Semi-Grand Ensemble for Salt

At fixed chemical potential for salt, the preceding constructions allow us to find all states of coexistence and the polymer and surfactant densities in them; below we create phase diagrams essentially by ‘joining the dots’ when these coexistences are plotted on the  $(\phi_b, \phi_p)$  plane. In most experiments, however, the experimenter fixes the total amount of salt (as well as that of bilayer and polymer) in the system. To deal with this is possible in principle, by a similar integration: the ion concentration obeys (16), so that defining the total salt concentration as  $n_s \equiv n_+$ , we have:

$$n_s = \frac{1}{D + \delta} \int_0^D n_i(x) dx = \frac{n_s^r}{D + \delta} \int_0^D e^{-eV(x)/T} dx \quad (13)$$

Equation (13) expresses the Donnan equilibrium for a lamellar phase [36, 37]: since  $V(x)$  is always positive for bilayers of finite separation, the total amount of salt  $n_s$  within a lamellar phase is smaller than in the the reservoir. This salt expulsion is more efficient, the closer together the bilayers, so that coexisting phases with different periods will contain different amounts of salt.

However, this additional calculation represents a major numerical complication. We have decided to neglect this, and thus work in a semi-grand ensemble with respect to salt. Experimentally our phase diagrams are those of a lamellar system in which a fixed volume of solvent, and fixed amounts of bilayer and polymer, are in contact with a salt reservoir through a dialysis membrane. This type of experiment is perfectly possible [36], but is not typical in studying polymer-doped lamellar phases. How the use of the salt reservoir affects our results will be discussed in Section 5.

### 4.4 Effect of Bilayer Surface Charge Density

With these considerations in mind, we now present phase diagrams from our model by mapping pairs of coexisting phase points. The error bars on the phase points result from the uncertainties associated with the graphical method by which coexistences were found, or, when this was very accurate, from the intrinsic accuracy of the numerics. The phase boundaries themselves have been drawn as guides for the eye and do not represent numerical fits to our data.

We study first the effect of changing the surface charge density,  $\sigma$ . Density–density phase diagrams, with polymer and bilayer volume fractions as composition variables, are shown in Fig. 8 for doped lamellar phases with  $\sigma = 0.05, 0.1$  and  $0.2 \text{ e nm}^{-2}$  (top, middle and bottom panels respectively). The middle phase diagram, calculated using the same parameters as Table 1, provides a reference for studying the influence of parameter variation on phase behaviour. All other phase diagrams are calculated by changing the parameter of interest above and below its reference value.

Results are shown for both coupled and uncoupled equations. In both cases, an increase in  $\sigma$  changes the phase diagram topology from a large area of  $L_\alpha L$  coexistence (top panel), through an intermediate “pinch off” region (middle panel, coupled case), to two miscibility gaps, separated by a single-phase  $L_\alpha$  region (middle panel, uncoupled; bottom panel). The  $L_\alpha L$  coexistence in

the “bilayer dilute” region of the phase diagram can be between the reservoir (isotropic phase) and polymer-free or polymer-loaded lamellar phases. At higher bilayer volume fractions, only  $L_\alpha L_\alpha$  coexistence between polymer-loaded lamellar phases is possible. Where the density difference between coexisting  $L_\alpha$  phases vanishes, critical points arise which close off the miscibility gaps; when this doesn’t happen the two phases are joined by a bottleneck of  $L_\alpha L_\alpha$  coexistence between loaded phases. At very high bilayer volume fractions,  $L_\alpha L_\alpha$  coexistence is between a polymer-loaded lamellar phase and one so concentrated as to contain no polymer.

The dielectric coupling, as could be expected, makes no difference at very low surface charge densities (top panel of Fig. 8). At intermediate  $\sigma$ , however, (middle panel) the topology of the phase diagram is coupling-dependent: in the coupled case, a characteristic neck joins two miscibility gaps, whilst in the uncoupled prediction the two gaps are already separate. At high  $\sigma$  (bottom panel) the same qualitative features are predicted for both approaches, but positions of phase boundaries and critical points are visibly affected. In particular, the coupled model predicts a dilute miscibility gap which is larger than in the uncoupled case.

The observed phase behaviour results from the interplay of polymer-induced attraction and electrostatic repulsion between the bilayers. The general features of this are not drastically modified the coupling. When  $\sigma$  is small, the polymer physics dominates the phase behaviour and drives  $L_\alpha L$  phase separation against a weak electrostatic repulsion, for polymer and bilayer concentrations which span a large region of the phase diagram. For higher values of  $\sigma$  the polymer attraction only dominates the electrostatic repulsion where this has decayed to sufficiently small values. Alternatively,  $L_\alpha L_\alpha$  phase separation can occur for concentrated bilayers, which confine the polymer solution and cause an attraction sufficient to partially compensate the electrostatic repulsion.

It was shown in Section 3.2 that including the dielectric coupling of the polymers affects both electrostatic repulsion, whose range is decreased, and the polymer-induced attraction, whose range is increased. For doped phases dilute in both bilayer and polymer, these changes clearly broaden the extent of the regions of phase separation (the pressure is more attractive over a greater range of intralamellar separations because of coupling). Thus, the miscibility gaps predicted by a model where electrostatics is coupled to polymer physics will be larger than in an uncoupled description. At high polymer and bilayer volume fractions, however, the range of the attraction and of the repulsion are different, and the coupled miscibility gap becomes smaller than the uncoupled prediction. This effect is discussed in more detail Section 4.7.

## 4.5 Effect of Reservoir Salt Content

Next we vary the salt concentration in the reservoir, to probe the effect of the screening of electrostatic interactions on the phase behaviour. Fig. 9 shows the density–density phase diagrams when the reservoir contains  $c_s^r = 0.047\text{M}$ ,  $0.02\text{M}$  and  $0.01\text{M}$  of salt (top, middle and bottom panels respectively; the middle panel is the same as in the previous figure).

The effect of increasing the screening length  $\lambda$  (decreasing salt) on phase diagram topology is similar to that of increasing  $\sigma$ . This is no surprise, since reducing the salt level increases the range of the electrostatic repulsion. The same general features arise: a large  $L_\alpha L$  region (top panel, coupled); its pinch-off, which is delayed by coupling terms (top panel, uncoupled; middle panel, coupled); and finally two opposing miscibility gaps (middle panel, uncoupled; bottom panel). The relative extent of the phase regions and their changes in shape (tieline length and tilt) evolves differently with  $c_s^r$  than with  $\sigma$ , however. For example, the miscibility gap in the dilute corner of the diagram shrinks in height as  $c_s^r$  decreases (middle to bottom panel), in contrast to Fig. 8.



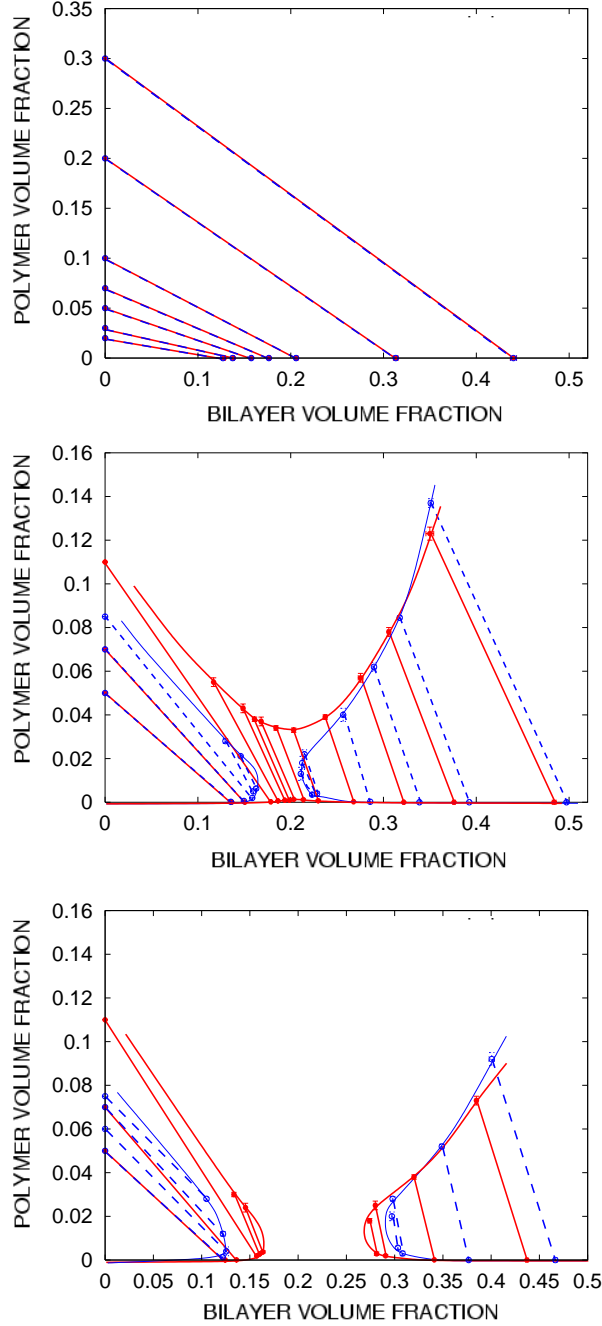


Figure 8: Effect of increasing surface charge density,  $\sigma$ , on the phase behaviour of a polymer-doped lamellar phase in contact with a salt reservoir. Top to bottom:  $\sigma = 0.05 \text{ e nm}^{-2}$ ,  $\sigma = 0.1 \text{ e nm}^{-2}$  and  $\sigma = 0.2 \text{ e nm}^{-2}$ . The coordinates of coexisting phases were found using the graphical method discussed in the text. Coupled ( $\bullet$ ) and uncoupled ( $\circ$ ) points, with associated error bars, mark these coordinates and have been connected by tielines (full and broken respectively). Approximate binodals have also been fitted through the points to highlight the shape of the miscibility gaps. Note that the vertical scale on the top diagram extends further than that of the other two.

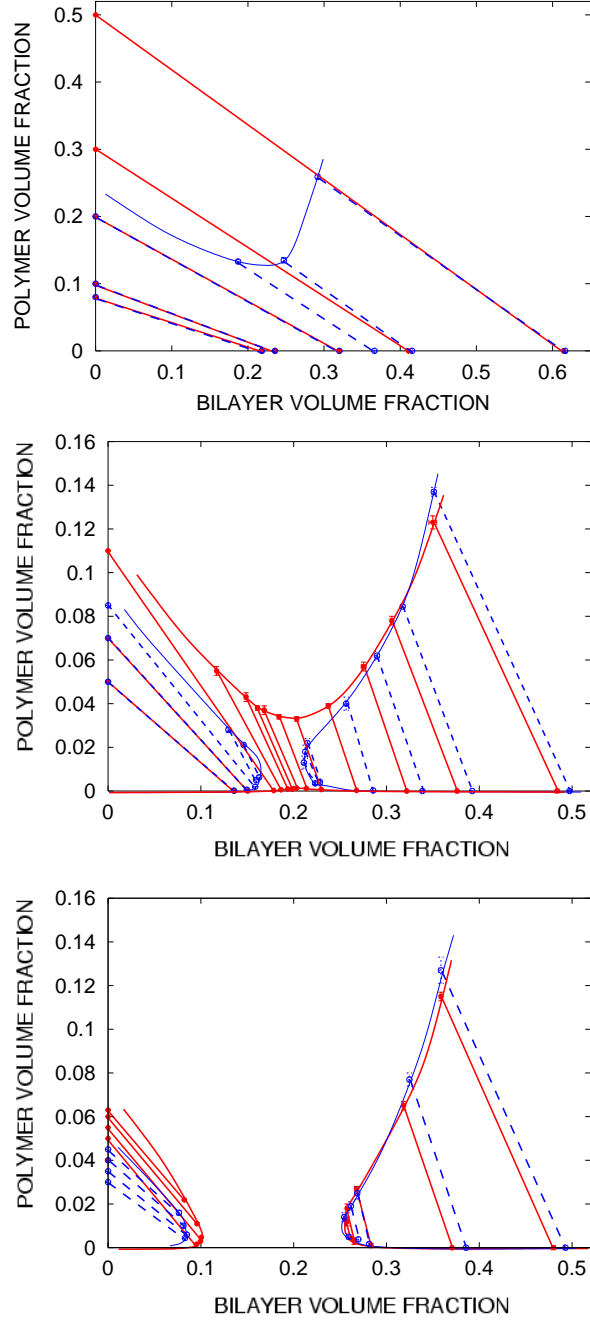


Figure 9: Effect of decreasing the reservoir salt concentration,  $c_s^r$ , on the phase behaviour of a polymer-doped lamellar phase. Top to bottom:  $c_s^r = 0.047$  M,  $c_s^r = 0.02$  M, and  $c_s^r = 0.01$  M. Methods and notation as in Figure 8. Note that the vertical scale on the top diagram extends further than that of the following two.

Just as for changes in  $\sigma$ , the dielectric coupling generally extends the coexistence regions for a given  $c_s^r$  compared to an uncoupled description. In the top panel,  $L_\alpha L$  coexistence is ubiquitous in the coupled predictions, whereas the uncoupled case shows  $L_\alpha L_\alpha$  coexistence beyond moderate bilayer concentrations. For  $c_s^r = 0.01M$  (bottom panel), in the concentrated miscibility gap, almost no differences between the two models are discernible (given the errors) in the phase boundary. The dilute coexistence region varies more markedly, and is larger in the coupled case.

The basic mechanism of phase separation, and the effect of coupling on this, was already described in the context of varying  $\sigma$ . Quantitative differences do arise because here we are now changing the range, as opposed to the magnitude, of the electrostatic repulsion. Dielectric coupling modifies electrostatic screening somewhat, and also alters the polymeric interaction by excluding monomers from regions of high field; these effects favour phase separation as stated previously.

#### 4.6 Effect of the Solution Flory Parameter

We now consider three different hypothetical polymers for which water is, respectively a poor solvent with  $\chi = 0.515$  (Fig. 10, top panel); a near *theta* solvent with  $\chi = 0.495$  (middle panel: the “reference” system, as in previous figures); and a good solvent with  $\chi = 0.3$  (bottom panel). Decreasing  $\chi$  in the range shown has broadly the same effect of an increase in  $\sigma$  or a decrease in  $c_s^r$ : merged  $L_\alpha L$  and  $L_\alpha L_\alpha$  regions (top panel) shrink (middle panel, coupled) and split into separate dilute and concentrated miscibility gaps (middle panel, uncoupled). Finally, the dilute miscibility gap disappears and only the concentrated gap is left (bottom panel). The general features of this phase evolution arise because a variation in the  $\chi$  parameter affects both the strength and range of the polymer interactions. Thus for poor and for *theta* solvents, the polymer solution can sense its confinement at large separations, so that bound lamellar phases are found in both dilute and concentrated regions. For a good solvent the range of the polymer-induced attraction is too short to cause phase separation in dilute samples so this is only effective at high concentration  $\phi_b$ .

The differences between coupled and uncoupled approaches are greater for the higher values of  $\chi = 0.515, 0.495$ . The top and middle panels of Fig. 10 show how the differences are more pronounced on the bilayer-dilute side of the phase diagram, where once again the coupling increases the extent of the  $L_\alpha L$  region with respect to the uncoupled case. However, for good solvents this miscibility gap is absent; and even for the miscibility gap at high concentration, coupling terms are swamped by the strong interaction between polymers. Hence no major differences in the coupled and uncoupled phase behaviour are detectable for  $\chi = 0.3$  (bottom panel).

#### 4.7 Effect of Dielectric Monomer Size

We now consider the role of  $\gamma$ , which governs the volume of polarisable material associated with a lattice monomer. Shown in Fig. 11 are the phase diagrams calculated when  $\gamma = 1.1$ ,  $\gamma = 1.5$  and  $\gamma = 2$ . As expected, an increase in  $\gamma$ , which implies a decrease of the amount of dielectric material in a polymer (see Fig. 2), reduces the difference between coupled and uncoupled approaches. When  $\gamma = 1.1$  (top panel), in the bilayer dilute region the  $L_\alpha L_\alpha$  coexistence predicted by the uncoupled model is replaced by a significantly larger area of  $L_\alpha L$  in the coupled case. However, for concentrated bilayer volume fractions, the coupled miscibility gap is smaller than the uncoupled one.

Note also that, even for  $\gamma = 2$  when there is a relatively small amount of dielectric material in each lattice monomer, there is still a strong effect on phase diagram topology near the pinch-off from one region of immiscibility to two. The phase diagram for these parameter values is topologically

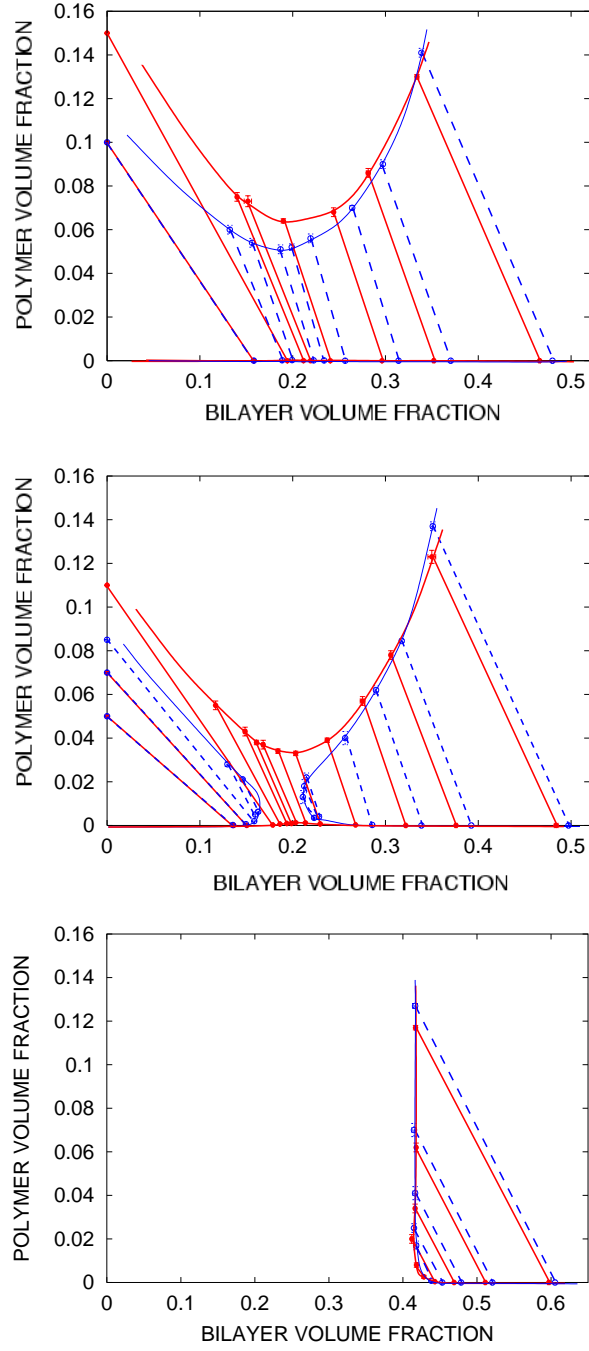


Figure 10: Effect of decreasing the  $\chi$ -parameter on the phase behaviour of a polymer-doped lamellar phase in contact with a salt reservoir. Top to bottom:  $\chi = 0.515$ ,  $\chi = 0.495$ , and  $\chi = 0.3$ . Method and symbols as in Fig. 8 Note that the horizontal scale of the bottom diagram extends further than that of the preceding two.

sensitive to all perturbations, including those arising from a relatively modest level of dielectric coupling between the polymeric and electrostatic interactions.

The differences between coupled and uncoupled predictions is generally as expected, with more dielectric material in a monomer (small  $\gamma$ ) giving larger enhancement of the miscibility gaps when coupling is added. However, at large  $\phi_b$  there appears to be an inversion in this trend (top panel), with the  $L_\alpha L_\alpha$  coexistence reduced with respect to the uncoupled predictions. This inversion (mentioned already in Section 4.4) results from the dielectric screening of highly confined polymers at moderate concentrations. To see this, consider a lamellar phase prepared at the composition marked by an  $X$  on the top panel of Fig. 9. In an uncoupled picture the compromise between electrostatic repulsion and polymer attraction can be achieved through phase separation, even though, at high concentration, the polymer attraction is of short range (the range involves the correlation length in the solution, which falls with increasing concentration [15]). In most parts of the phase diagram, introducing coupling enhances the polymer-mediated attraction by keeping polymers away from the high field regions close to the bilayers (Section 4.4), but in this regime that tendency is largely overcome by the high polymer osmotic pressure. Instead, the polymers between layers help to screen the electrostatic repulsion (by reducing the dielectric constant) and this stabilizes the lamellar phase against phase separation to a state of small  $D$ .

## 5 Discussion

We now discuss the relation between the phase diagrams found above and those obtained experimentally for polymer-doped smectics. Because of the various approximations made (including the assumptions of strongly non-adsorbing polymer and of a mean-field approach, and neglect of all interaction terms between bilayers other than the electrostatic and polymer-mediated forces) we focus on qualitative rather than quantitative comparisons.

### 5.1 Differences Due to the Salt Reservoir

We first must decide whether the use of a salt reservoir (Section 4.3) in our calculations affects the qualitative aspects of our predictions. Recall typical experiments on polymer-doped lamellar phases are performed by adding a fixed amount of salt to each sample. When lamellar phases contact a reservoir through a semipermeable membrane, they can expel salt into the reservoir (the Donnan effect [36, 37]) reducing the repulsion between them. For a system of fixed salt content, however, this expulsion is not possible. This implies a greater electrostatic repulsion between bilayers, so that more polymer will be required to cause phase separation in a fixed salt system. We thus expect the shape of the phase diagrams (and the tilt of the tielines) to differ from our Semi-Grand ensemble predictions, but expect the general qualitative features and their dependence on parameter variation to be the same.

### 5.2 Comparison with Experimental Results

Our results reproduce several of the main qualitative features observed in experiments on polymer-doped lamellar phases, notably  $L_\alpha L_\alpha$  and  $L_\alpha L$  phase separations (see e.g [10, 12, 13, 14, 30, 17]). However we do not capture all the features of very dilute and very concentrated lamellar phases. For example, an experimentally observed  $L_\alpha L$  coexistence involving very concentrated lamellar phases is not predicted in our phase diagrams. Another feature which does not appear in our results is

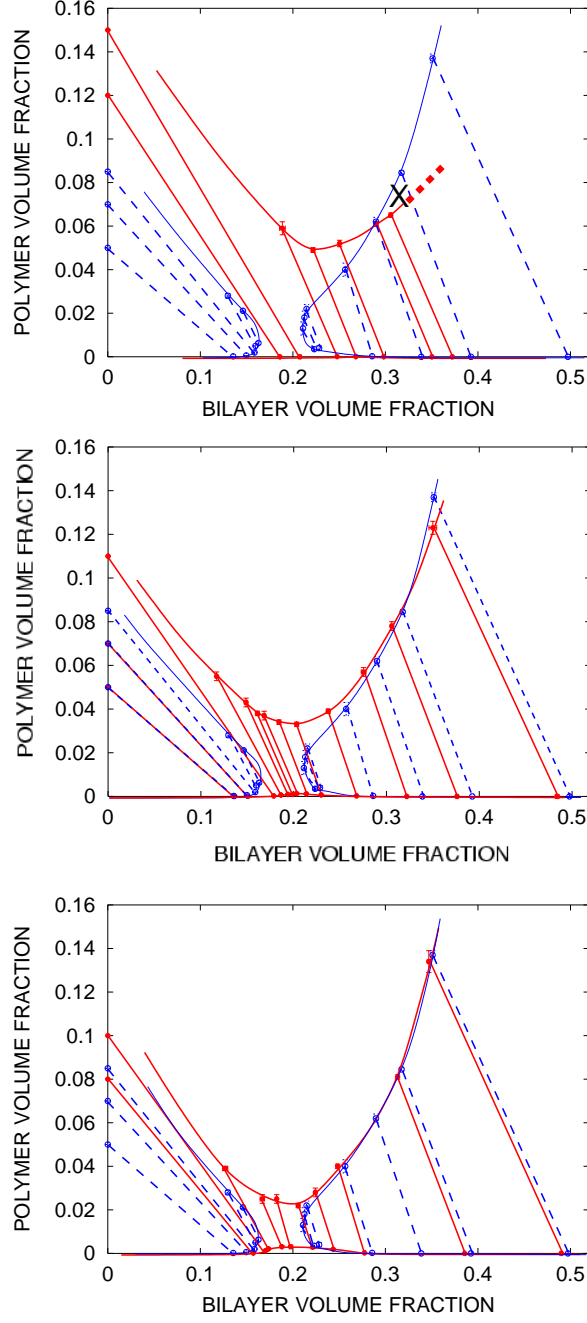


Figure 11: Effect of increasing the dielectric size factor  $\gamma$  on the phase behaviour of a polymer-doped lamellar phase in contact with a salt reservoir. Top to bottom:  $\gamma = 1.1$ ,  $\gamma = 1.5$ , and  $\gamma = 2$ . Method and notation as in Fig. 8. For  $\gamma = 1.1$  in the coupled case, our method did not allow obtain the phase behaviour in the region of concentrated bilayers. The dotted line indicates what we believe to be a reasonable extrapolation of the binodal. Point  $X$  is referred to in the text.

the “closed-loop” miscibility gap sometimes observed [10, 12]. This has been ascribed to the two different ranges of the repulsive interactions between bilayers: the very short range of hydration and the larger range of electrostatics [16]. Such repulsions compete with polymer induced attraction at different separations between bilayers. For large bilayer volume fractions (small separations) the phase separation terminates where the hydration force dominates the polymer attraction. The same thing happens at small bilayer volume fractions (large separations), where electrostatic repulsion dominates the polymer attraction. These considerations, if Sear’s model [16] is correct, explain why a model with no short ranged repulsion such as ours cannot predict closed loops, but only open regions of phase coexistence terminating in a critical point.

Our phase diagrams predict qualitatively correct trends when electrostatic parameters, such as salt concentration and surface charge density are changed. Ligoure et al. have investigated these changes experimentally by looking at the phase behaviour of doped lamellar phases of fixed polymer content. They found that progressive addition of salt [13, 14] or reduction of surface charge density [30, 17] cause a transition from a single phase lamellar sample to a  $L_\alpha L_\alpha$  coexistence. These qualitative trends agree with our predictions, e.g. of a system with  $\phi_b = 0.2, \phi_p = 0.02$  as  $\sigma$  is decreased from 0.2 (Fig. 8, bottom panel) to  $0.1 \text{ e nm}^{-2}$  (middle panel). The reduction of the surface charge density induces the same  $L_\alpha L_\alpha$  transition as observed in experiment.

The experimentally confirmed trends reported seem largely insensitive to the question of whether the dielectric coupling of the polymer-mediated and electrostatic interactions is included. As shown above, this is mainly a quantitative rather than a qualitative difference, so long as the evolution of phase diagrams is considered in the round. However, this does not preclude large differences when coupled and uncoupled results are compared for particular parameter values, particularly around the pinch-off point where the immiscible region splits into two pieces (Fig.8, etc.).

## 6 Conclusions

Our results show that the dielectric proprieties of uncharged polymers confined between charged surfaces couple together electrostatic and polymeric effects in a non-additive fashion, which can have significant quantitative impact on phase diagrams. Since the monomers in a chain are electrically polarised by the (nonuniform) electric field of the double layer, the depletion of polymers close to the surface is electrostatically enhanced. Conversely, the polarisation of the monomers provides an additional source of screening of the electrostatics. Consequently, the osmotic interaction between surfaces as a function of distance is also affected: the range of the electrostatic part of the interaction is effectively reduced with respect to a model which ignores coupling, whereas that of the depletion attraction is effectively increased.

Our results, based on a mean-field theory that couples both sorts of interaction, gives a good account of the phase behaviour of polymer-doped lamellar phases. Our study of its evolution under parameter variation confirms that the coupling effects do not drastically alter the trends from the uncoupled case but do alter the quantitative predictions; near topological changes in phase diagram, but not elsewhere, these quantitative corrections change the qualitative behaviour. Coupled and uncoupled predictions differ most under the following conditions (i) moderately high surface charge densities (since strong polarisation of the polymers requires high fields); (ii) marginal solvency, i.e., near-*theta* conditions (where the response in polymer concentration to external energy shifts is maximized); and (iii) polymers containing a large volume of low dielectric material (for obvious reasons of coupling strength). On the other hand, coupling effects were not discernible for lamellar

phases with small surface charges, those doped with polymers residing in a good solvent, or chains with insufficient dielectric contrast.

Future experimental investigations could perhaps put these coupling effects more strongly in evidence. For example, it would be interesting to compare the phase behaviour of lamellar phases doped with polymers of strongly contrasting dielectric properties (changing either the monomeric dielectric contrast and/or dielectric volume) under matched conditions of near-*theta* solvency. Alternatively, instead of investigating the phase behaviour, a more direct test of the interplay between polymeric and electrostatic interactions could be performed by directly measuring the force between charged surfaces across a polymer solution using a surface force apparatus, as in [19]. From a theoretical point of view, it might also be of interest to consider the consequences of dielectric coupling for the interaction between curved surfaces, such as those of colloids (within the Derjaguin approximation [38] it is easy to apply our model to this situation), as has been done by Borukhov et al. [5] in the case of charged surfaces interacting across a solution of polyelectrolytes. It might also be of interest to consider kinetic processes, where coupling effects should be less subtle, such as the diffusion of a dielectric polymer onto a charged surface. More generally we hope our work will stimulate further experiments on the nonadditivity of electrostatic and depletion interactions in the presence of dielectric contrast.

## Acknowledgement

This work was funded in part under EPSRC Grant GR/S10377/01.

## A Derivation of Model Equations and Osmotic Pressure

Equations (6) and (7) follow from the null variations of the free energy action Equation (1). For this purpose it is convenient to write Equation (1) fully:

$$\begin{aligned} \mathcal{F}_\Omega[V, n_i, \phi] &= \int_\Gamma f_\Omega(V, n_i, \phi) d\mathbf{r} = \\ &= \int_\Gamma \left( -\frac{1}{2} \epsilon_e(\phi) (\nabla V)^2 + \sum_{i=+,-} n_i q_i V + T \sum_{i=+,-} n_i (\ln n_i - 1) - \sum_{i=+,-} \mu_i n_i + \right. \\ &\quad \left. + \frac{T}{a^3} \left[ \frac{\phi}{N} (\ln \frac{\phi}{N} - 1) + (1 - \phi) \ln(1 - \phi) + \chi \phi (1 - \phi) - \frac{\mu_p}{T} \right] + \frac{T}{36a} \frac{(\nabla \phi)^2}{\phi} \right) d\mathbf{r} \end{aligned} \quad (14)$$

Note that the ideal contribution to the polymer free energy differs here from the standard Flory–Huggins expression by an extra term  $\phi/N$  (we follow the convention of [23]). The term is linear in  $\phi$ , and so is inconsequential to any derived quantity.

### A.1 The Modified Poisson–Boltzmann Equation

Performing a variation with respect to the electrostatic potential, we set:  $\delta \mathcal{F}_\Omega / \delta V = 0$  or, equivalently,  $\frac{\partial f_\Omega}{\partial V} - \nabla \frac{\partial f_\Omega}{\partial \nabla V} = 0$ . From this we recover the Maxwell equation:

$$\nabla(\epsilon_e(\phi) \nabla V) = - \sum_{i=+,-} n_i q_i \quad (15)$$



where  $\epsilon_e(\phi)$  is given by Equation (5).

Similarly a variation with respect to the ion number density  $\delta\mathcal{F}_\Omega/\delta n_j = 0$ , i.e.  $\frac{\partial f_\Omega}{\partial n_j} - \nabla \frac{\partial f_\Omega}{\partial \nabla n_j} = 0$  yields the Boltzmann factor for ion concentrations:

$$n_i = n_i^r e^{-q_i V/T} \quad (16)$$

where,  $n_i^r \equiv e^{-\mu_i/T}$  defines the chemical potential  $\mu_i$  of ion  $i$ , fixed by the reservoir. All symbols in (15) and (16) have also been previously defined. Substituting Equation (16) into (15) yields a modified Poisson–Boltzmann equation in  $V$ :

$$\nabla(\epsilon_e(\phi)\nabla V) = - \sum_{i=+,-} n_i^r q_i e^{-q_i V/T} \quad (17)$$

which, in the case of monovalent ions, becomes (6).

## A.2 The Polymer Equation

A variation with respect to the polymer volume fraction  $\delta\mathcal{F}_\Omega/\delta\phi = 0$ , i.e.  $\frac{\partial f_\Omega}{\partial\phi} - \nabla \frac{\partial f_\Omega}{\partial \nabla\phi} = 0$ , yields:

$$\begin{aligned} -\frac{1}{2} \frac{d\epsilon_e}{d\phi} (\nabla V)^2 &+ \frac{T}{a^3} \left[ \frac{1}{N} \ln \frac{\phi}{N} - \ln(1-\phi) - 1 + \chi - 2\chi\phi - \frac{\mu_p}{T} \right] + \\ &- \frac{T}{36a} \left[ 2 \frac{\nabla^2 \phi}{\phi} - \left( \frac{\nabla \phi}{\phi} \right)^2 \right] = 0 \end{aligned} \quad (18)$$

This describes the response of the polymer concentration to external perturbations such as electric fields and confining hard boundaries. When such perturbations are not present, we recover a uniform polymer solution (the reservoir). In this case  $\phi = \phi^r$ , and Equation (18) fixes the chemical potential of the solution:

$$\frac{\mu_p}{T} = \left[ \frac{1}{N} \ln \frac{\phi^r}{N} - \ln(1-\phi^r) - 1 + \chi - 2\chi\phi^r \right] \quad (19)$$

To simplify Equation (18) we change variable to  $\psi \equiv \phi^{1/2}$ . This implies  $2\nabla^2 \phi/\phi - (\nabla \phi/\phi)^2 = 4\nabla^2 \psi/\psi$ . Thus, substituting (19) into (18) and carrying out the differentiation of the Maxwell–Garnett relation (5) for  $\epsilon_e$  we obtain:

$$\begin{aligned} \frac{1}{2} \frac{3K\alpha\epsilon_1}{(1+K\alpha\psi^2)^2} (\nabla V)^2 &+ \frac{T}{a^3} \left[ \frac{1}{N} \ln \left( \frac{\psi^2}{\psi^{r2}} \right) - \ln \left( \frac{1-\psi^2}{1-\psi^{r2}} \right) - 2\chi(\psi^2 - \psi^{r2}) \right] + \\ &- \frac{T}{9a} \frac{\nabla^2 \psi}{\psi} = 0 \end{aligned}$$

which is easily rearranged into Equation (7).

## A.3 Osmotic Pressure from a Conservation Law

In mechanics, when the Lagrangian (density) does not explicitly depend on time, the Hamiltonian is a constant of the motion [20]. Similarly, the free energy action density of our model does not explicitly depend on position; we can thus define the following conserved quantity:

$$\mathcal{H} \equiv \sum_m p_m \nabla Q_m - f_\Omega = \text{const.} \quad (20)$$

where  $f_\Omega$  is the free energy action density defined by (14), and  $Q_m$  and  $p_m$  are, respectively, the generalised coordinates and momenta of the problem. The generalised momenta, defined as  $p_m \equiv \frac{\partial f_\Omega}{\partial \nabla Q_m}$ , are:

$$p_{n_i} = \frac{\partial f_\Omega}{\partial \nabla n_i} = 0 \quad (21)$$

$$p_\phi = \frac{\partial f_\Omega}{\partial \nabla \phi} = \frac{2T}{36a} \frac{\nabla \phi}{\phi} \quad (22)$$

$$p_V = \frac{\partial f_\Omega}{\partial \nabla V} = -\epsilon(\phi_d) \nabla V \quad (23)$$

so that by (20) we can define the following quantity:

$$\begin{aligned} \mathcal{H} &= p_V \nabla V + p_\phi \nabla \phi - f_\Omega = \\ &= -\frac{1}{2} \epsilon_e(\phi) (\nabla V)^2 - \sum_{i=+,-} n_i q_i V - T \sum_{i=+,-} n_i (\ln n_i - 1) + \sum_{i=+,-} \mu_i n_i + \\ &- \frac{T}{a^3} \left[ \frac{\phi}{N} (\ln \frac{\phi}{N} - 1) + (1 - \phi) \ln(1 - \phi) + \chi \phi (1 - \phi) - \frac{\mu_p}{T} \right] + \frac{T}{36a} \frac{(\nabla \phi)^2}{\phi} = \text{const.} \end{aligned}$$

Upon substitution of (19) for the polymer chemical potential and (16) for the ion densities, (24) becomes, after a few algebraic manipulations:

$$\begin{aligned} \mathcal{H} &= -\frac{1}{2} \epsilon_e(\phi) (\nabla V)^2 + T \sum_{i=+,-} n_i^r e^{-q_i V/T} + \\ &- \frac{T}{a^3} \left[ \frac{\phi}{N} (\ln \frac{\phi}{\phi^r} - 1) - \phi \ln \left( \frac{1 - \phi}{1 - \phi^r} \right) + \chi \phi (2\phi^r - \phi) + \phi + \ln(1 - \phi) \right] + \\ &+ \frac{T}{36a} \frac{(\nabla \phi)^2}{\phi} = \text{const.} \end{aligned} \quad (24)$$

The total stress on a surface in an ionic solution in the vicinity of a charged surface has osmotic and electrostatic contributions which can be calculated from a stress tensor (the Maxwell stress tensor with an added isotropic osmotic contribution, see Podgornik in [1]). The normal component of this stress,  $\Sigma_{xx}$  is identical with the first two terms, the electrostatic and ionic contributions respectively, of Equation (24). The other terms represent the contributions to  $\Sigma_{xx}$  due to the polymer solution. Hence we identify  $\mathcal{H}$  with  $\Sigma_{xx}$ . On the midplane ( $x = D/2$ ) the electrostatic contribution vanishes by symmetry, as do all gradient terms. Here (only) the conserved quantity  $\Sigma_{xx}$  can be identified with the osmotic pressure  $\Pi$ , which has ionic and polymeric contributions.

### Reservoir Pressure and Net Osmotic Pressure

In the reservoir we have an ideal ionic solution mixed with a Flory–Huggins polymer solution, and no net field contributions. When evaluated in the “reservoir limit” (as we did when deriving the chemical potential), we thus expect the mid-plane osmotic pressure (24) to reduce to the sum of Van’t Hoff ideal contribution for the ions and a Flory–Huggins pressure term for the polymer solution. Setting  $V = 0 = \nabla V$  and  $\phi = \phi^r$ , (24) becomes:

$$\Pi^r = T \sum_{i=+,-} n_i^r + \frac{T}{a^3} \left[ \frac{\phi^r}{N} - \chi \phi^{r^2} - \phi^r - \ln(1 - \phi^r) \right] \quad (25)$$

Equation (25) agrees with our expectations and is an expression for the reservoir pressure. It also provides a check of our derivation of  $\Sigma_{xx}$  as a conserved quantity, since the polymer contribution to Equation (25) can be independently and directly derived by differentiation of the Flory–Huggins free energy of a bulk polymer solution (e.g.: see section III.1.3 of Reference [15]).

To find the net force per unit area between the plates, we need to subtract the reservoir osmotic pressure (25) from the midplane osmotic pressure  $\Pi$  which is numerically equal to the conserved quantity defined in (24):

$$\begin{aligned}\Pi^{net} &= \Pi - \Pi^r \\ &= -\frac{1}{2}\epsilon_e(\phi)(\nabla V)^2 + T \sum_{i=+,-} n_i^r (e^{-q_i V/T} - 1) + \\ &\quad - \frac{T}{a^3} \left[ \frac{\phi}{N} \ln \frac{\phi}{\phi^r} + \frac{(\phi^r - \phi)}{N} + (1 - \phi) \ln \left( \frac{1 - \phi}{1 - \phi^r} \right) - \chi(\phi^r - \phi)^2 - (\phi^r - \phi) \right] + \\ &\quad + \frac{T}{36a} \frac{(\nabla \phi)^2}{\phi} = \text{const.}\end{aligned}\tag{26}$$

In principle the net force per unit area could be found by evaluating the (conserved) right hand side at any position  $x$  between the plates. If we assume monovalent ions, (26) becomes:

$$\begin{aligned}\Pi^{net} &= -\frac{1}{2}\epsilon_e(\phi)(\nabla V)^2 + 4n_s^r T \sinh^2 \left( \frac{eV}{2T} \right) + \\ &\quad - \frac{T}{a^3} \left[ \frac{\phi}{N} \ln \frac{\phi}{\phi^r} + \frac{(\phi^r - \phi)}{N} + (1 - \phi) \ln \left( \frac{1 - \phi}{1 - \phi^r} \right) - \chi(\phi^r - \phi)^2 - (\phi^r - \phi) \right] + \\ &\quad + \frac{T}{36a} \frac{(\nabla \phi)^2}{\phi} = \text{const.}\end{aligned}\tag{27}$$

For the case under study of opposing flat surfaces, the electric field and all gradient terms vanish at the midplane by symmetry; choosing this as the place to evaluate the right hand side, (27) reduces to Equation (10).

## References

- [1] Holm, C.; Kékicheff, P.; Podgornik, R., Eds.; *Electrostatic Effects in Soft Matter and Biophysics*; Kluwer: Dordrecht, Boston and London, 2001.
- [2] Menes, R.; Pincus, P. A.; Stein, B. *Phys. Rev. E* **2000**, *62*, 2981-2984.
- [3] Netz, R. R. *Eur. Phys. J. E* **2000**, *3*, 131-141.
- [4] Russel, W. B.; Saville, D. A.; Schowalter, W. R. *Colloidal Dispersions*; Cambridge University press: Cambridge, 1989.
- [5] Borukhov, I.; Andelman, D.; Orland, H. *J. Phys. Chem. B* **1999**, *103*, 5042-5057.
- [6] Perutz, M. F. *Science* **1978**, *201*, 1187-1191.
- [7] Kötzt, J.; Kosmella, S. *Curr. Opin. Colloid Interface Sci.* **1999**, *4*, 348-353.

- [8] Radlinska, E. Z.; Gulik-Krzywicki, T.; Lafuma, F.; Langevin, D.; Urbach, W.; Williams, C. E. *J. Phys. II France* **1997**, 7, 1393-1416.
- [9] Radlinska, E. Z.; Gulik-Krzywicki, T.; Lafuma, F.; Langevin, D.; Urbach, W.; Williams, C. E.; Ober, R. *Phys. Rev. Lett.* **1995**, 74, 4237-4240.
- [10] Ficheux, M.-F.; Bellocq, A.-M.; Nallet, F. *J. Phys. II France* **1995**, 5, 823-834.
- [11] Ficheux, M.-F.; Bellocq, A.-M.; Nallet, F. *Colloid. Surf. A* **1997**, 123, 253-263.
- [12] Javierre, I.; Bellocq, A.-M.; Nallet, F. *Langmuir* **2001**, 17, 5417-5425.
- [13] Ligoure, C.; Bouglet, G.; Porte, G. *Phys. Rev. Lett.* **1993**, 71, 3600-3603.
- [14] Ligoure, C.; Bouglet, G.; Porte, G.; Diat, O. *J. Phys. II France* **1997**, 7, 473-491.
- [15] De-Gennes, P.-G. *Scaling Concepts in Polymer Physics*; Cornell University Press: Ithaca and London, 1991.
- [16] Sear, R. P. cond-mat/9709205.
- [17] Porcar, L.; Marignan, J.; Ligoure, C. *Langmuir* **2000**, 16, 2581-2594.
- [18] Zhang, K.; Linse, P. *J. Phys. Chem.* **1995**, 99, 9130-9135.
- [19] Freyssingeas, E.; Antelmi, D.; Kélicheff, P.; Richetti, P.; Bellocq, A.-M. *Eur. Phys. J. B* **1999**, 9, 123-136.
- [20] Schwinger, J. S.; Deraad, L. L.; Milton, K. A.; Tsai, W.-Y. *Classical Electrodynamics*; Perseus Book Group: Reading, Mass., 1998.
- [21] Cahn, J. W.; Hilliard, J. E. *Journal of Chemical physics* **1958**, 28, 258-267.
- [22] Doi, M. *Introduction to Polymer Physics*; Oxford University Press: Oxford, 1996.
- [23] Pagonabarraga, I.; Cates, M. E. *Europhys. Lett.* **2001**, 55, 348-354.
- [24] Note that some authors use a coefficient where the numerical factor 36 in the denominator of the SG coefficient is replaced by 24. This corresponds to a use of the small wavelength limit of the free energy expansion in the RPA [23].
- [25] Sihvola, A. H. *Electromagnetic mixing formulas and applications*; IEE: London, 1999.
- [26] Landau, L. D.; Lifshitz, E. *Electrodynamics of Continuous Media*; Pergamon Press: Oxford, 1960.
- [27] Sipe, J. E.; Boyd, R. W. *Phys. Rev. A* **1992**, 46, 1614-1629.
- [28] Netz, R. R.; Andelman, D. *Phys. Reports* **2003**, 380, 1-95.
- [29] Landau, L. D.; Lifshitz, E. M. *Statistical Physics, Part 1*; Pergamon Press: Oxford, 1980.
- [30] Ligoure, C.; Bouglet, G.; Porte, G.; Diat, O. *J. Phys. II France* **1997**, 7, 493-501.

- [31] This choice of parameters entails that the condition  $\lambda \gg R \gg a\phi^{-1/3}$  discussed in Section 2.1 is marginally satisfied at best.
- [32] Cosgrove, T.; Fleer, G. J.; Stuart, M. A. C.; Scheutjens, J. M.; Vincent, B. *Polymers at Interfaces*; Kluwer Academic Publishers: Englewood Cliffs NJ, 1993.
- [33] Press, W. H.; Teukolsky, S. A.; Vetterling, W. T.; Flannery, B. P. *Numerical recipes in C++: the art of scientific computing*; Cambridge University Press: New York, 2002.
- [34] Teraoka, I.; Wang, Y. *J. Chem. Phys.* **2001**, *115*, 1105-1114.
- [35] Brooks, J. T.; Cates, M. E. *J. Chem. Phys.* **1993**, *99*, 5467-5480.
- [36] Dubois, M.; T., Z.; Belloni, L.; Delville, A.; Levitz, P.; Setton, R. *J. Chem. Phys* **1992**, *96*, 2278-2286.
- [37] Donnan, F. G. *Chem. Rev.* **1924**, *1*, 73.
- [38] Safran, S. A. *Statistical Thermodynamics of Surfaces, Interfaces and Membranes*; Addison-Wesley: New York, 1994.